BTGNX: AN ACOUSTIC BENCHMARK WIND TUNNEL EXPERIMENT FOR TIP-GAP NOISE

Fabian REUSCHLING[1], Lev LIBERSON[2], Michael POTT-POLLENSKE[1], Jan W. DELFS[1], Daniel ERNST[3]

[1] *German Aerospace Center (DLR), Institute of Aerodynamics and Flow Technology, Technical Acoustics, Lilienthalplatz 7, 38108 Braunschweig, Germany*

[2] *previously: German Aerospace Center (DLR), Institute of Aerodynamics and Flow Technology, Technical Acoustics, Lilienthalplatz 7, 38108 Braunschweig, Germany*

[3] *German Aerospace Center (DLR), Institute of Aerodynamics and Flow Technology, Experimental Methods, Bunsenstrasse 10, 37073 Göttingen, Germany*

SUMMARY

Within a current cooperation between the fan manufacturer ebm-papst and the department of Technical Acoustics at the DLR-Institute of Aerodynamics and Flow Technology, an optimisation workflow for a fan blade side edge geometry to minimise tip-gap noise is being developed. For validation of this approach, an acoustics-focused wind tunnel experiment was performed. It employs extensive near- and far-field acoustic measurement techniques and is intended to serve as a benchmark experiment for future tip-gap noise research.

INTRODUCTION

With the reduction of other noise sources in housed fans, the tip-gap noise originating from the gap between a fan blade's side edge and the fan housing has become increasingly relevant for the overall sound radiated by a fan. The analysis of this noise source and development of sound reduction measures is the topic of a current cooperation between the fan manufacturer ebm-papst and the department of Technical Acoustics at the DLR-Institute of Aerodynamics and Flow Technology. The ultimate goal is the development of a numerical optimisation workflow for the geometry of the fan blade's side edge (for details see [1]). For this purpose, the simulations have to be able to accurately determine the relative difference in sound radiated by two different side edge geometries. Literature data to be used for validation of this approach is scarce, however. Therefore, the Braunschweig Tip-Gap-Noise eXperiment (BTGNX) was developed within the cooperation

with the aim of providing a broad database that can be used not only for validation of the optimisation workflow, but also serve as a benchmark for future tip-gap noise research.

EXPERIMENTAL SET-UP

For the set-up of the validation experiment, cues were drawn from previous tip-gap noise experiments (e.g. [2], [3]). Representative for these is a thorough – aerodynamics focused – investigation carried out at the University of Lyon [4]. This used a static wing with a NACA 5510 aerofoil and 200 mm chord, mounted vertically between two plates extending the wind tunnel nozzle. The tip-gap is created between the wing side edge and one of the plates. These experiments usually have several shortcomings from an aeroacoustic perspective. The most significant one being the use of relatively small wind tunnels leading to a small wing span – in case of the experiment performed in Lyon 200 mm in the no-gap configuration – and potential influences of the mounting on the opposite side of the tip-gap on the measured far-field spectra. The small span also makes sound source localization using phased microphone arrays difficult.

The goal of the Braunschweig Tip-Gap-Noise eXperiment was to address these shortcomings. It was set-up in the Acoustic Wind tunnel Braunschweig (AWB) featuring an 800 mm wide and 1200 mm tall nozzle exit surface. While the basic set-up, the used aerofoil, and chord are identical to the experiment carried out at the University of Lyon, the wing span was extended to 700 mm in the no-gap configuration. The tip-gap (height h) is created between the wing's side edge and a flat plate mounted horizontally in the wind tunnel (see Figure 1). The last 30 mm of the wing span were made interchangeable to study the effect of different wing tip geometries. Four different winglets were manufactured using Stereolithography (SLA) 3D-printing: A simple extension of the wing's aerofoil as reference winglet (0), a winglet rounded off from the pressure to the suction side (1), a winglet where this rounding extends beyond the suction side edge (2) and a winglet with extensions on the suction and the pressure side creating the shape of a "T" (3). The rotation point of the wing was placed 30 mm (0.15 chord) downstream of the leading edge on the camber line. This position ensures that the tip vortex system remains at the same position throughout all measured angles of attack and was determined from PIV measurements performed in the experiment at the University of Lyon. The flow on the bottom side of the plate was tripped directly after the leading edge. The flow on the wing was not tripped. This set-up better separates the noise generated in the tip-gap and from the mounting of the wing compared to previous experiments in small wind tunnels.

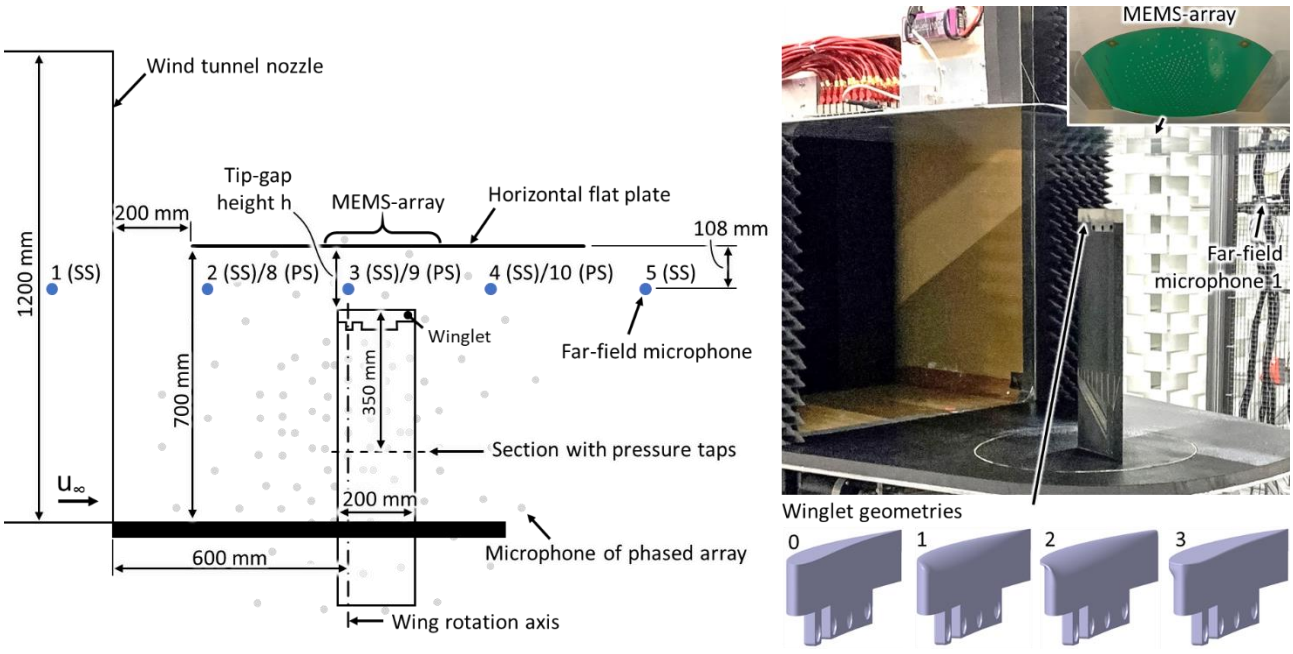

Figure 1: Set-up of the Braunschweig Tip-Gap-Noise eXperiment

The wing was equipped with 31 static pressure taps along the mid-span section (i.e. at 350 mm from the side edge) and two Kulites type LQ-062 behind 0.5 mm pinholes, one in the Pressure Side (PS) at 0.25 chord and one in the Suction Side (SS) at 0.9 chord, both at 33 mm from the wing side edge. A further two Kulites type XCQ-093 were integrated into the side edge of the reference wingtip on the camber line at 0.03 chord and 0.775 chord. To capture the far-field acoustics, ten ¼" microphones (type GRAS 46BF-1) were placed 108 mm below the flat plate, spaced at an angle of 12° relative to rotation point of the wing. Seven of the microphones were located on the suction side, starting with an angle of -24° measured towards a line perpendicular to the primary flow direction. The remaining three microphones were placed on the pressure side directly opposite to the microphone positions 2, 3 and 4 (-12°, 0°, 12°) on the suction side. The microphones had a distance of 1.7 m to the middle plane of the wind tunnel nozzle, except for the last two microphones on the suction side (at 36° and 48°) which had a distance of 2.67 m. A phased microphone array with 96 ½" microphones was placed on the suction side in a distance of 1.7 m from the nozzle middle plane. The middle was located 473 mm below the flat plate and at the same distance from the nozzle as the wing rotation point. Finally, an array consisting of 256 MEMS microphones (MEMS = Micro Electro-Mechanical System) was integrated into the flat plate opposite the wing's side edge. A detailed description of this array and measurement results are reported in [5].

In the measurement campaign, 22 gap heights between 0 mm (no gap) and 200 mm (presumed to be equivalent to a free side edge) and nine geometric angles of attack between 0° and 16° in 2° intervals were measured. The reference winglet was measured at inflow velocities of 30 m/s, 40 m/s, 50 m/s and 60 m/s. The other three winglets were measured at velocities of 40 m/s and 60 m/s. The microphone data were recorded at a sample rate of 51 kHz over a period of 30 seconds.

RESULTS AND DISCUSSION

While the primary purpose of the dataset is to be post-processed for validation of the simulations, an analysis of the measured spectra for the reference configuration – 40 m/s inflow velocity (u_∞) and 12° geometric angle of attack (α_{geo}, equalling about 5.9° aerodynamic angle of attack) – is still conducted for far-field microphone 4 (located at a 90° angle to the chord) to gain an understanding of the occurring effects. The two most important parameter variations in this regard are the variation of the gap height to identify the most relevant frequency bands and the comparison between the four winglet geometries to draw conclusions about the prevalent sound generation mechanisms. All presented Sound Pressure Levels (SPLs) are normalised to a distance of 1.7 mm from the wing's rotation axis.

Gap height variation

The far-field sound pressure spectra for the most relevant gap heights (h) at the reference configuration are presented in Figure 2. Additionally, a measurement for the same set-up except for the wing is included as background noise. The spectra for all measured gap heights can be found in Figure 6 in the Annex.

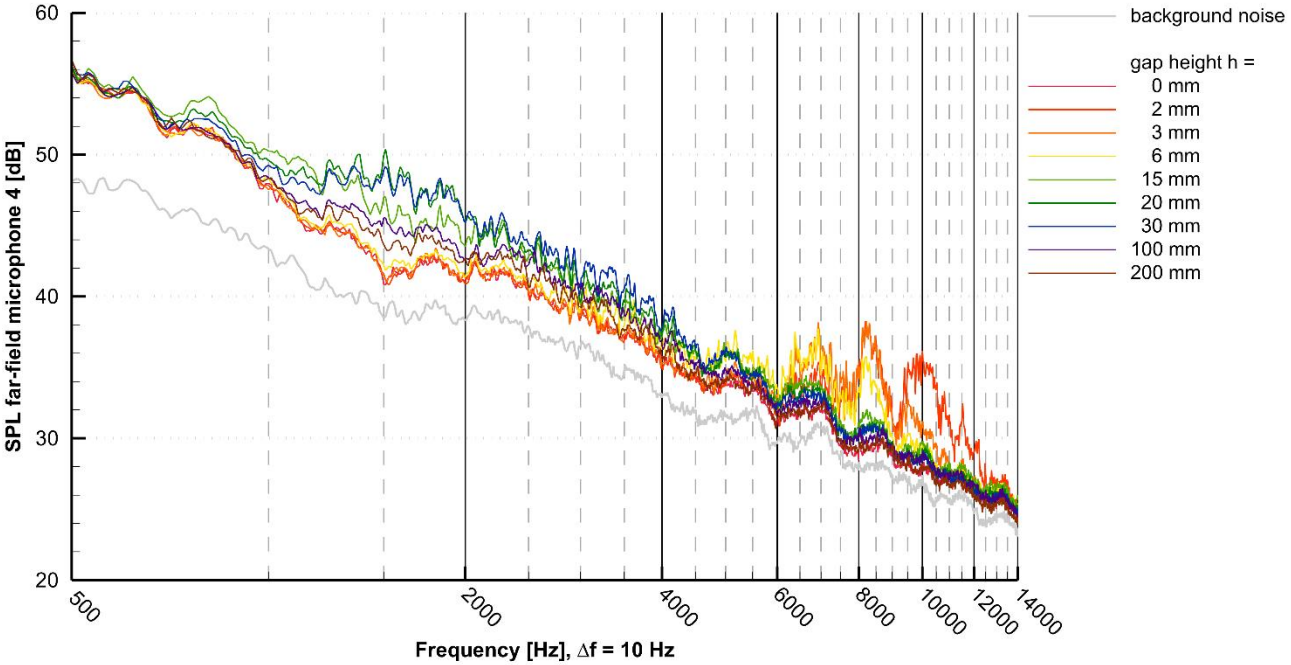

Figure 2: SPL for far-field microphone 4 at selected gap heights (reference winglet, u_∞ = 40 m/s, α_{geo} = 12°)

From the spectra, two frequency bands can be distinguished where a change in gap height leads to a change in the recorded sound pressure level: The first is between 1 kHz and 3 kHz where the spectra fan out and the second is between 6 kHz and 12 kHz where three broadband peaks are observed. In the first frequency band, the lowest SPLs are measured for gap heights up to 6 mm, thereafter gradually increasing by 9 dB in total to the maximum at 20 mm gap height. This is followed by a reduction that levels out 4 dB above the lowest SPLs at 100 mm gap height. Consequently, the spectra at gap heights above 100 mm can be considered not to be influenced by the tip-gap noise source any more, confirming the presumption of a free side edge at 200 mm gap height. The minimal difference in sound pressure level between gap heights up to 6 mm coincides with the boundary layer thickness at this location on the flat plate, which was measured to be 8 mm at 40 m/s inflow velocity. When the gap height is equivalent to the boundary layer thickness the measured SPL is equivalent to that of the free side edge (see Figure 6). This indicates that the tip-gap noise source is suppressed when the wing's side edge is within the boundary layer of the flat plate. The observation is confirmed by the sound source localization using the phased microphone array that primarily shows secondary sound sources at 2 mm gap height (in this case the mounting of the wing in the bottom side plate) whereas a clear source in the tip-gap region is visible for 20 mm gap height (see Figure 3).

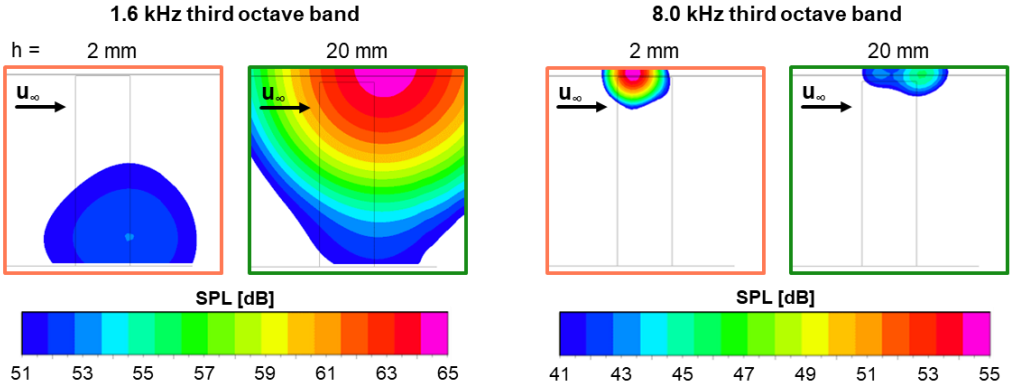

Figure 3: Sound source localization in 1.6 kHz and 8.0 kHz third octave bands (reference winglet, u_∞ = 40 m/s, α_{geo} = 12°, conventional beamforming)

In the second frequency band between 6 kHz and 12 kHz on the contrary, the tip-gap noise is the strongest at small gap heights with the maximum being 8 dB above the free side edge at h = 2 mm. The following decline in measured sound pressure level is the largest at the third peak around 10 kHz and less strong and occurs at larger gaps heights at the other two peaks around 7 kHz and 8 kHz. At 20 mm gap height, the SPL is close to that of the free side edge. Until this gap height, the source localization places the primary source in the tip-gap near the leading edge of the wing. At larger gap heights, the primary source shifts to the tip of the trailing edge indicating a non-tip-gap-related sound generation mechanism (see Figure 3). The sound source at 0 mm and 1 mm gap height is also placed in the tip-gap, albeit the SPL being at the level of the free side edge. This is likely due to how these two gap heights were measured: In order to prevent scratching along the MEMS-array, measurements at 0 mm gap height (direct contact) and 1 mm gap height were taken separately, while all other gap heights were measured in one motion starting at h = 2 mm.

Winglet variation

To draw more detailed conclusions about the sound generation mechanisms present in the two identified frequency bands, it is helpful to compare the sound pressure levels for the four winglet geometries at gap heights of 2 mm, 6 mm, 20 mm and 100 mm. The respective spectra for the reference configuration and far-field microphone 4 are presented in Figure 4. Each of the winglets with geometry modifications compared to the reference winglet was designed to reduce one of the tip-gap noise generation mechanisms known from literature [6]: The winglet rounded off from the pressure to the suctions side aims at weakening the Tip Separation Vortex (TSV) typically rolling up on the wing's side edge, the T-shaped winglet aims to push the Tip Leakage Vortex (TLV) further from the wing's suction side to reduce the noise generated as it convects past the trailing edge, and the winglet where the rounding extends past the suction side combines both approaches.

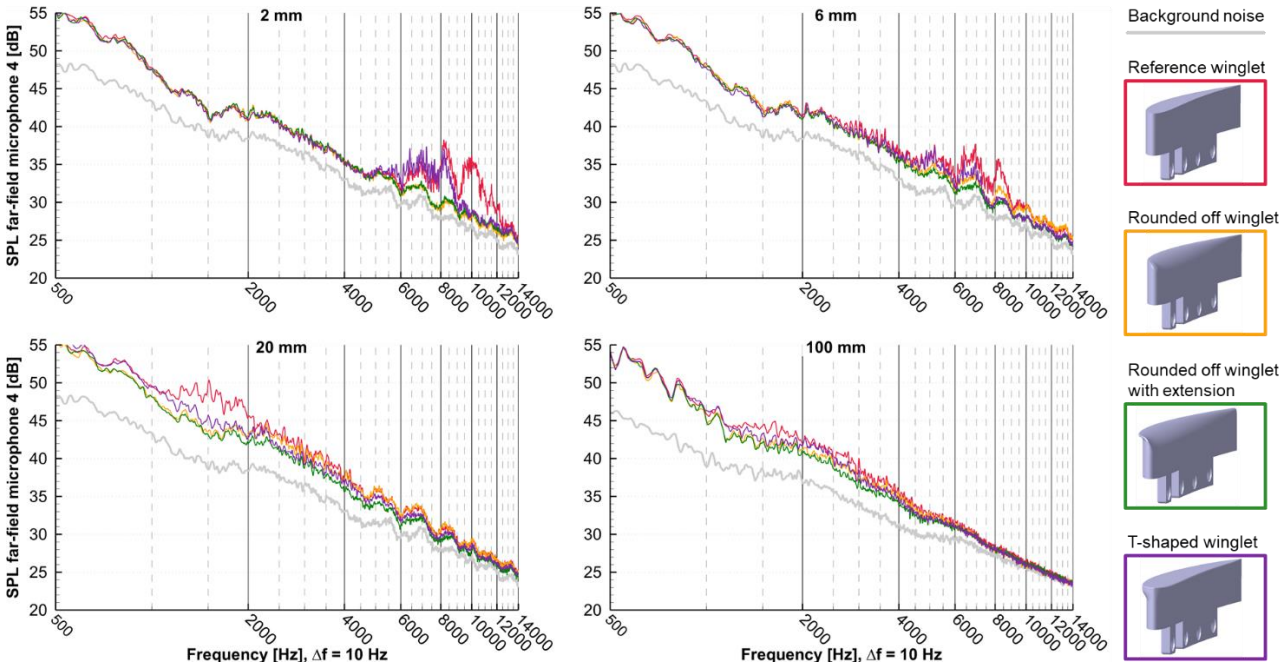

Figure 4: SPL for far-field microphone 4 for different winglet geometries (u_∞ = 40 m/s, α_{geo} = 12°)

In the first frequency band between 1 kHz and 3 kHz, no effect of the winglet geometry on the measured sound pressure level is observed at gap heights below the boundary layer thickness (2 mm and 6 mm). This is in line with the previously drawn conclusion that the tip-gap noise source is suppressed if the wing's side edge is within the boundary layer. At 20 mm gap height, all modified winglet geometries lead to a SPL reduction – up to 7 dB for the two rounded off winglets and 5 dB for the T-winglet – compared to the reference winglet. This difference gradually becomes smaller towards larger gap heights. It is not clear which sound generation mechanism is prevalent in this

frequency band, as all geometry modifications lead to a reduction in radiated sound. It can be suspected that the primary cause of sound is the TSV since both winglets rounded off from the pressure to the suctions side (preventing the roll up of the tip separation vortex) lead to similar SPL reductions. However, it is unclear then why the T-shaped winglet also causes a reduction in radiated sound compared to the reference winglet. One possible explanation is the larger TSV-reattachment zone (see [7]) due to the wider side edge. Confirmation might be achieved from the analysis of the surface pressures measured with the MEMS-array that are not considered in this work.

Between 6 kHz and 12 kHz, the largest differences between the winglets are found for 2 mm gap height, as is expected from the analysis of the gap height variation. The three broadband peaks at 7 kHz, 8 kHz, and 10 kHz are only observed for the reference winglet. The spectrum of the T-winglet includes the first two peaks, while no clear peak is found in the spectra of the rounded off winglets. The recorded sound pressure levels for these winglets are roughly equal and up to 7 dB below those of the reference and the T-winglet. At 6 mm gap height, this difference narrows and the spectrum of the T-winglet shifts towards the one for the rounded off winglet with extension. The opposite behaviour is observed for the spectrum of the rounded off winglet that moves closer to that of the reference winglet. This trend continues towards larger gap heights. From 20 mm gap height, the spectra of the reference and the rounded off winglets overlay, as do those of the T-winglet and the rounded off winglet with extension. This shift indicates two different sound generation mechanisms in the second frequency band: At gap heights up to 6 mm, the primary cause is the tip separation vortex scraping off the pressure side edge which is not observed for the two rounded off winglets. The sound source localisation near the leading edge (discussed in the analysis of the gap height variation) coincides well with where the TSV starts forming according to literature [8]. Towards larger gap heights, the main cause becomes the tip leakage vortex interacting with the trailing edge. As the rounded off winglet with extension and the T-winglet push the TLV further from the wing, the radiated sound is reduced compared to the other two winglets. This conclusion also fits the previously discussed sound source localisation.

POST-PROCESSING FOR COMPARISON WITH NUMERICS

As stated previously, the goal of the numerical investigations running in parallel is to accurately predict the relative differences between the noise generated by the winglets to facilitate a geometry optimisation (for results see [1] and [9]). Part of the optimisation workflow is the calculation of an acoustic metric that is used to place the investigated winglet geometries in a sequence from loudest to quietest. To validate this step of the workflow, the measured data are post-processed in a similar way yielding one sequence of winglets for each combination of inflow velocity, gap height and angle of attack (“configuration”).

The processing is performed automatically for the entire dataset of far-field microphone measurements on the basis of third octave bands. In a first step, the background noise is subtracted from the sound pressure level in each frequency band. Then, the resulting SPLs are summed up over the two frequency ranges determined from the gap height variation (1 - 3 kHz and 6 - 12 kHz) and the entire range from 1 kHz to 12 kHz. Subsequently, the sequence of winglets is determined from the summed-up SPLs. Both, the subtraction of the background noise and the summation of the SPLs is done with arithmetic subtraction/addition as well as energetically to investigate the robustness of the approach.

The resulting number of occurrences of each sequence of winglets per far-field microphone is plotted in Figure 5. Each row corresponds to one calculation scheme (arithmetic/energetic subtraction/addition) in the three frequency ranges while each column represents one sequence of winglets (from loudest to quietest). The cells are coloured according to the number of occurrences of the respective sequence in the entire measurement dataset. In total, 103 configurations with valid data for all four winglets were found.

Figure 5: Occurrences of winglet sequences
Calculation schemes: 1 – arithmetic subtraction of background noise, arithmetic summation; 2 – arithmetic subtraction, energetic addition; 3 – energetic subtraction, arithmetic summation; 4 – energetic subtraction, energetic summation

For the two frequency bands from 1 kHz to 3 kHz and from 6 kHz to 12 kHz, there generally is good agreement between the different calculation schemes. The sole exception is found for far-field microphone 6. This, however, is due to significant noise in the microphone's spectra masking the tip-gap noise. When the combined frequency range is used, the most common sequence strongly depends on the calculation scheme. This is explained by the different effects and trends previously found for the two frequency bands, preventing the determination of a common sequence and underlining the importance of considering both frequency bands independently. Overall, the sequence calculation is found to be robust and independent from how the single value used to sort the winglets is calculated.

Analysing the found sequences, the previously discovered distinction between the two frequency bands is visible: Between 1 kHz and 3 kHz, the two most common sequences place the reference winglet as loudest, followed by the rounded off, the rounded off with extension and the T-winglet (sequence 2) or the T-winglet, the rounded off and the rounded off with extension (sequence 3). Between 6 kHz and 12 kHz, the most common sequence also starts with the reference winglet and the rounded off winglet, but is then followed by the T-winglet and the rounded off with extension as quietest winglet (sequence 1). This sequence is rarely found in the first frequency band. The other two often observed sequences in the second frequency band are sequence 2 – already detected between 1 kHz and 3 kHz – and the rounded off winglet as loudest, followed by the reference winglet, the rounded off with extension and the T-winglet (sequence 4). For both frequency bands, a directivity can be observed. Between 1 kHz and 3 kHz, sequence 3 is more commonly observed than sequence 2 the further downstream the microphone is placed on the suction and the pressure side (i.e. the rounded off winglet with extension being the quietest instead of the T-winglet). In the second frequency band (6 – 12 kHz), a shift from sequence 2 to sequence 1 (i.e. also from the T-winglet to the rounded off with extension as the quietest winglet) is observed, but less clearly and only on the suction side.

Comparing the calculated sequences to those found in analysing the winglet variation, many similarities are found. In the first frequency band, sequence 3 is clearly observed starting with a gap

height of 20 mm, while it can be suspected that sequence 2 is deduced from small gap heights where there is little difference in the SPL of the four winglet geometries. Between 6 kHz and 12 kHz, the winglet sequence found for gap heights larger than 20 mm – reference and rounded off winglets at about the same level and rounded off with extension and T-winglet at lower SPLs – is mirrored in sequences 1 and 2. However, the winglet sequence found for gap heights below 20 mm (equivalating to sequence 3 or sequence 5 with the last two winglets switching places) is rarely observed in the calculated sequences, while sequence 4 cannot be seen in the winglet variation analysed previously. A closer inspection reveals that sequences 3 and 5 are only prevalent among gap heights below 20 mm at inflow velocities of 40 m/s. At inflow velocities of 60 m/s, the spectra in this frequency band are closer together and sequence 4 more commonly observed. Consequently, the sequence found for the first frequency band in the previous section is less important when the entire dataset is considered.

In summary, the post-processing approach is well suited to validate the numerical optimisation workflow. The trends and winglet sequences present in the measured data are captured and can easily be compared to those deduced from the acoustic metric. Moreover, analysis of the sequences leads to a better understanding of the measured data and can be used to place observations made for one particular configuration into context. The same post-processing approach was used to find common gap height sequences, generally confirming the conclusions drawn from the gap height variation studied herein.

CONCLUSION AND OUTLOOK

In this work, the set-up of a benchmark experiment for tip-gap noise and far-field results for a tip-gap height and wing side edge variation were presented. The design is based on previous tip-gap noise experiments using a vertically mounted non-rotating wing, but incorporates modifications to limit the influence of secondary noise source enabling a better separation of the tip-gap noise source. From the sound pressure levels measured for the gap height variation, two distinct frequency bands were identified in which the tip-gap noise source is active. In the first band between 1 kHz and 3 kHz, the noise source is suppressed at gap heights below the boundary layer thickness and strongest at 20 mm gap height. From comparison of the wing side edge modifications, it is suspected that the sound generated by the tip separation vortex when scraping off the pressure side edge and reattaching on the wing side edge is dominating in this frequency band. However, further investigation using the surface pressures recorded with a MEMS-array installed in the tip-gap opposite of the wing's side edge (reported in [5]) is necessary. In the second frequency band between 6 kHz and 12 kHz, the strongest contribution of the tip-gap noise source to the far-field was recorded for 2 mm gap height. Analysis of the side edge modifications revealed the separation of the TSV as the primary noise source at gap heights below the boundary layer thickness. At larger gap heights, the interaction of the tip leakage vortex was identified as the prevalent noise source.

Finally, the wing side edge modifications were sequenced from loudest to quietest for all measured configurations (i.e. combinations of inflow velocity, gap height and angle of attack). This revealed the reference side edge (straight continuation of the aerofoil) to be the loudest in both frequency bands. In the first band, it is followed by the T-shaped side edge and the side edges rounded off from the pressure to the suction side. In the second band, the rounded off side edge is louder than the T-shaped side edge followed by the rounded off side edge extending slightly beyond the suction side. The results confirmed that the effects observed in the spectra for the reference configuration (u_∞ = 40 m/s, α_{geo} = 12°) are also present in the other measured configurations. Besides giving a concise overview of all measured data, the sequences can be used to evaluate the numerical optimization workflow that is based on the prediction of relative differences between different side edge geometries.

Future work will focus on correlating the acoustic effects measured in this experiment with the aerodynamic data reported for other tip-gap noise experiments (e.g. the research performed at the University of Lyon, extensively reported in [4]). Furthermore, a detailed analysis of other measured configurations will be performed, attempting to link the conclusions drawn to findings reported in literature, in particular a recently published research by Awasthi et al. [10] investigating the radiated sound at different ratios of gap height to boundary layer thickness. This was found to be a major obstacle for comparison with previous research as the boundary layer thickness usually was much larger than the largest gap height investigated.

ACKNOWLEDGEMENTS

The authors would like to thank the cooperation partners at ebm-papst for the fruitful cooperation, helpful input, and support throughout the project.

BIBLIOGRAPHY

[1] L. Liberson, F. Reuschling, R. Ewert, M. Pott-Pollenske, J. W. Delfs – *BTGNX: Windkanalexperiment zu kopfspaltströmungsinduzierter Geräuschentstehung – Teil 1: Numerische Ergebnisse*. Fortschritte der Akustik – DAGA 2024, **2024**

[2] M. C. Jacob, J. Grilliat, R. Camussi, G. Caputi Gennaro – *Aeroacoustic investigation of a single airfoil tip leakage flow*. International Journal of aeroacoustics, volume 9, number 3, **2010**

[3] I. Saraceno, S. Palleja-Cabre, C. Paruchuri, B. Ganapathisubramani – *Influence of non-dimensional parameters on the tip leakage noise*. AIAA Aviation Forum 2023, **2023**

[4] J. Grillant– *Contribution à l'étude aéroacoustique des écoulements de jeu.* PhD Thesis, **2009**

[5] D. Ernst, C. Spehr, F. Reuschling, M. Schneider – *BTGNX: A MEMS microphone array for the acoustic benchmark wind tunnel experiment for tip-gap noise.* Proceedings of Fan Noise 2025 Symposium, **2025**

[6] R. Koch, M. Sanjosé, S. Moreau – *Large-Eddy Simulation of a Single Airfoil Tip-Leakage Flow.* AIAA Journal, volume 59, number 7, **2021**

[7] J. D. Denton – *Loss mechanisms in Turbomachines.* Proceedings of the ASME 1993 International Gas Turbine and Aeroengine Congress and Exposition, volume 2, **1993**

[8] S. Kang, C. H. Hirsch – *Experimental study on the three-dimensional flow within a compressor cascade with tip clearance: Part II—the tip leakage vortex.* ASME Journal of Turbomachinery, **1993**

[9] P. Dietrich, S. R. Mallu, F. Lex – N*umerical investigation of different wing tip geometries on the acoustics of an airfoil with tip gap in a wind tunnel.* Proceedings of Fan Noise 2025 Symposium, **2025**

[10] M. Awasthi, A. O. Wills, D. Moreau, P. Croaker, P. Dylejko – *A Parametric Study of Far-Field Sound Radiated by an Idealised Tip Leakage Flow.* 30th AIAA/CEAS Aeroacoustics Conference, **2024**

ANNEX

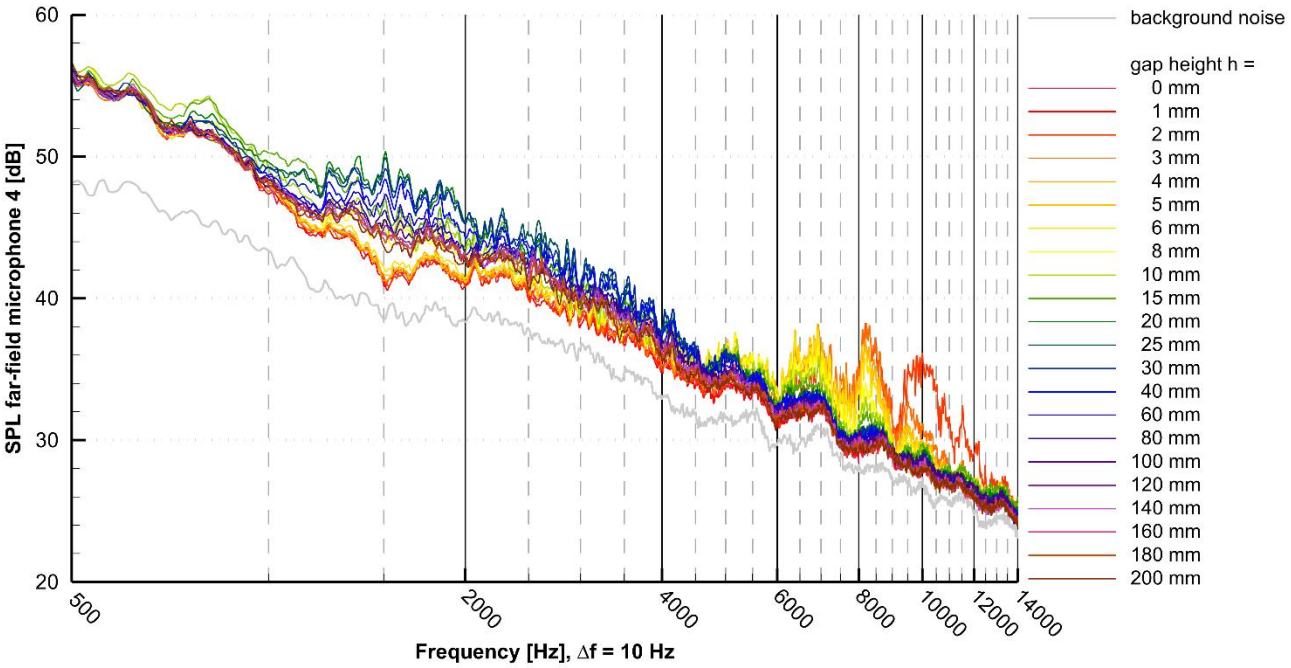

Figure 6: SPL for far-field microphone 4 at all measured gap heights (reference winglet, u_∞ = 40 m/s, α_{geo} = 12°)